Available online at www.sciencedirect.com

ScienceDirect

Procedia Computer Science 85 (2016) 362 – 369

Procedia Computer Science

International Conference on Computational Modeling and Security (CMS 2016)

A new method of brain tissues segmentation from MRI with accuracy estimation

Sudipta Roy [a*], Samir Kumar Bandyopadhyay[b]

[a]*Department of Computer Science and Engineering, Academy of Technology, Adisaptagram, Hooghly-712121, West Bengal, India*
[b]*Department of Computer Science and Engineering, Technology Campus, Calcutta University, JD-2, Sector-III, Salt Lake, Kolkata-98, India*

Abstract

In this paper, a new concept has been incorporated using level set methodology for the specific segmentation of brain tissues in magnetic resonance imaging (MRI) brain images. In this segmentation, the normal tissues such as WM (White Matter), GM (Gray Matter) and CSF (Cerebrospinal Fluid) with other part of human head such as skull, marrow, and muscular skin are segmented. The segmentation has been done by using repeated level set method based on the condition sharp peak greater than three. The each segmented component is generating a hierarchical structure to make correct tissue segmentation. The performance of the segmentation method is estimated by different accuracy, sensitivity and error correction metric. The performance of segmentation process is analyzed using a defined set of MRI brain. From visualization and mathematical both point of measurement proposed gives very superior results on brain MR images.

Peer-review under responsibility of the Organizing Committee of CMS 2016

Keywords: Brain Tissues, MRI of brain, Segmentation, Abnormality, Accuracy Estimation, Level Set, Performance Measurement.

1. Introduction

Databases surround hundreds of cross-sectional and longitudinal MRI which might require several hours per scan for correct manual segmentation. Such segmentation may have several error and exhibit nontrivial intra-expert inconsistency in the segmentation of huge databases over weeks which is known as “rater drift” [1].

* Corresponding author. Tel.: +91-9432514700
*E-mail address:*sudiptaroy01@yahoo.com

Peer-review under responsibility of the Organizing Committee of CMS 2016
doi:10.1016/j.procs.2016.05.244

Furthermore, manual segmentation using the transverse, coronal and sagittal views may result in uneven boundaries, which cause difficulties in character analysis. Hence, the fact that many applications depend on accurate, robust and cost-effective brain segmentation has inspired much work for developing automatic brain segmentation tools. The challenge in brain MRI segmentation is due to issues such as noise, non-uniform intensity, partial volume effect, shape complexity and natural tissue intensity variations. Under such conditions, incorporation of a priori medical knowledge, commonly represented in anatomical brain atlases by state-of-the-art studies is essential for robust and accurate automatic segmentation.

Several brain tissue segmentation approaches have been projected over the years. Some proposals attempt to use clustering techniques, being the Expectation Maximization a popular method. Some of those utilize Markov Random Fields to add perspective of the neighborhood of the voxel being labeled [2] [3]. In [2], an earlier probability atlas is engaged to initialize the EM method which gives spatial information. However, other authors have also proposed segmentation methods more debesides CSF, GM or WM, like the basal ganglia, brainstem and others [4] [5]. Recently, discriminative semantic segmentation [6] method based on supervised decision forest to segment the brain tissues that achieving good results. Potential of diagnosing and differentiating diseases using MR images formulate them suitable in developing new pharmacotherapeutic methods [7-8]. Segmentation is a most important issue in processing and analyzing MR images which impress the ultimate results of analysis. Automatic segmentation of brain MR Images into its major tissues remains an inextricable problem in domain of medical image processing. First of all, noise may modify the gray value of pixels which uncertain the segmentation results. Moreover, in-homogeneities in MR Images modify the gray value of pixels belonging to one tissue increasingly and thus it makes difficult to their segmentation. Furthermore, the restriction on image resolution directed to partial volume effect in which one voxel may include parts from more than one tissue. Other imaging artifacts such as calibration parameters also make segmentation of MR Images more difficult [9]. The main limitation of existing segmentation to extract normal and abnormal tissue of brain and skull is the accuracy. We have found the problems which include: (a) the subcortical gray matter is underestimated, especially around the thalamus, the white matter fibers enter the gray matter structures, leading to poor contrast in the MR image. Accurate non-rigid alignment and segmentation are extremely difficult in this region. (b) The cortical gray matter is overestimated because segmenting the small folds of cortical gray matter correctly is more complicated with a probability atlas. Its smooth borders increase the likelihood of bridges or cavities across adjacent banks of a sulcus and influence the segmentation towards an overestimation of cortical gray matter [10]. (c) Over or under segmentation of normal brain tissue and non brain part are performed by the existing segmentation methodology. d) Increasing number of structures in the segmentation problem also increases the problem's statistical complexity and likelihood of misclassified voxels.

The rest of the paper is organized as follows. In Section II, proposed method has been described briefly. Detailed results from proposed method are provided in Section III as results and discussion section. Finally we conclude our method in Section IV.

2. Proposed Method

We have to perform the three stage level set segmentation with three membership functions that clearly find out three regions. But for significant accurate segmentation of different tissues of brain and non brain part we use the repetitive level set segmentation method. The repetition of segmentation has been depends on the number of sharp peaks of the segmented region. We will repeat our three phase level set for peak greater than three for every segmented region. We have chosen peak value three because core module of our proposed method used concepts of three region segmentation.

The elementary conception of level set is to completely evolve a higher dimensional function $\Phi: \Omega \to R$ whose zero level set $C: \Phi = 0$ represents dynamic shapes on the surfaces. The growing curve C partitions the image into two regions: C_{in} region inside the curve, which is enclosed by $\Phi > 0$ and C_{out}, which is the region outside the curve, i.e., where $\Phi < 0$. Thus the entire idea behind [11] this steps is to represent the closed curve C defined on the image domain can be represented by the zero level set $\Phi(x, y) = 0$ of a higher dimensional function called a Lipschitz function $\Phi: \Omega \to R$ such that

$$\Phi(x,y)=\begin{cases}=0 & at\ C\ (x,y)\epsilon\ \Omega\\ >0 & inside\ C(x,y)\epsilon\ \Omega\\ <0 & outside\ \ C(x,y)\epsilon\ \Omega\end{cases} \quad (1)$$

The curve C changes by $\partial_t C = F.N$ where F is derived from generic energy function of the speed of evolution, and N indicated as the outside unit normal vector to the growing curve C. The associated evolution proposed by *Oshar and Sethian* [11] of the level set function then be represented by $\partial_t \Phi = F.|\nabla\Phi|$. Unfortunately, these models are highly sensitive to noise, which makes them unsuitable for medical images as these images are usually noisy and contain obscure, ill-defined boundaries. We used regularization of $H(\Phi)$ using $C^2(\Omega)$ functions for computing the associated Euler-Lagrange equation, as proposed in [12-13], Using the Heaviside function H and Dirac delta function δ, minimizing the regularized energy functional with respect to Φ gives the associated Euler-Lagrange equation. Parameterization by an artificial time t≥0 gives the following update equation of $\Phi(x,y,t)$ in the descent direction:

$$\frac{\partial\Phi(x,y,t)}{\partial t}=\delta_\epsilon(\Phi)\left[\mu.div\left(\frac{\nabla\Phi}{|\nabla\Phi|}\right)-v+L_{12}\sum_{i=1}^{M_1}w_i g\left((x,y)\middle|\mu_i,\sum_i\right)\times P(C_{in})\right.$$
$$\left.-L_{21}\sum_{j=1}^{M_2}w_j g\left((x,y)\middle|\mu_j,\sum_j\right)\times P(C_{out})\right] \quad (2)$$

w_i; i = 1……M, represent mixture weights or prior probabilities of each component satisfying summation of all weight equals to one for M pieces Gaussian densities. The initial outline is defined by $\Phi(x,y,0)=\Phi_0(x,y)$. A Gaussian mixture model can be represented as a weighted sum of M pieces Gaussian densities,

$$P(X|\lambda)=\sum_{i=1}^{M}w_i g(X|\mu_i,\sum_i) \quad (3)$$

Where $X=\{x_1,x_2,x_3,\ldots..,x_n\}$ is a set of N observations from a D dimensional space, w_i, i=1,2,…,M represent mixture weights or prior probabilities of each module satisfying $\sum_{i=1}^{M} w_i = 1$;$g(x_j|\mu_j,\sum_j)$ are D-variate Gaussian modules and denote the probability of observation x_j coming from the i^{th} component. Each Gaussian module can be represented as:

$$g\left(x_j\middle|\mu_i,\sum_i\right)=\frac{1}{(2\pi)^{D/2}|\sum_i|^{1/2}}\exp\left\{-\frac{1}{2}\left(x_j-\mu_i\right)'\sum_j^{-1}(x_j-\mu_i)\right\} \quad (4)$$

Where $\mu_i,\sum_i$ are the representation mean and covariance matrices of individual modules. Hence, the parameters of the model are given by $\lambda=\{w_i,\mu_i,\sum_i\}$, i=1,2,….,M. The model parameters can be estimated by maximizing the overall likelihood of the observations X coming from the model λ. Maximum likelihood phrase is a non-linear function of the parameters λ and, therefore, a closed form solution for direct maximization is not possible.

The histogram of a digital image with L of total probable intensity levels in the range [0,G] is defined as the discrete function:

$$h(r_k)=n_k \quad (5)$$

Where r_k is the k^{th} intensity level in the interval [0,G] and n_k is the number of pixels in the image whose intensity level is r_k. 255 is the maximum possible value for G for gray scale image. The process of peak calculation is made by choosing preceding three and next three neighbour positions for each gray value k in a circular manner into (k-3)(k-2), (k-1), (k+1), (k+2) and (k+3) respectively. If the frequency of a gray value *k* is larger than that of its three adjacent left and three adjacent right gray value frequencies then *k* is identified as a peak (p_k). Sharp peak

frequency is calculated from the total number of peaks value recorded from above divided by three. When segmentation method stopped after applying above method, we use expect maxima (EM) to extract maximum area between two connected regions of brain, and maximum area always appear as left child. If we consider a binary tree of root is the input image (BI) itself then we segment it into two regions BI1(contains WM, GM, marrow, and muscles skull) and BI2(contains GM, CSF, muscles skull). Inputted brain image is treated as level 0 and BI1 and BI2 treated as level 1. Number of sharp peak greater than 3 at level 1, so we repeat the segmentation and the segmented region of level 1 produce the level 2. Segmented part of level 2 does not have any sharp peak greater than 3 for normal brain. For the entire segmented region we place maximum area as left child. Region BI12 and BI21 both contains GM and muscles skull, so we add this segmented region to improve the accuracy. Region BI11 contains WM and marrow, and BI22 contains CSF and fats. Finally we segment WM, marrow, GM, muscles skull, CSF, and fats by using max area from left to right. If any abnormality present we can detect it in level 2, all steps are remain same except we use abnormality extraction methodology [14] and rest of the region are treated as normal segmented tissue.

3. Results and Discussion

We tested our method with a couple of MRI of brain images [15] from brainweb standard dataset. Our method correctly segment for different category of MRI of brain. The outputs of different steps of our proposed methodology with almost perfect segmentation for transverse type MRI has been describe here. It should be noted that all parameters that appear in the method have been set to fixed values, so all results shown here have been achieved with the same parameters. The results of different steps we used in our methodology shown in Fig. 1 below. Fig. 1(b) is the output generated by level set segmentation on Fig. 1(a) is test MRI of brain image. When we segment according to the level set method, it is very clearly visible to us that some of segmented parts are overlapped in each region of segmentation. To remove this problem we have incorporated the concepts of sharp peak on segmented image. That means we need to repeat the level set in each segmented region to produce better results or output. Thus reapply level set as segmented region has number of sharp peak greater than three to get better accuracy. Fig. 1(c) and Fig. 1(d) are the results of level set segmentation applied on segmented part of Fig. 1(b). Fig.1(c) consists of WM, some amount of GM, marrow, and few amount of muscle skin. Fig. 1(d) consists of CSF, some amount of GM, and muscle skin. Now, the number of sharp peaks of segmented parts of Fig. 1(c) and Fig 1(d) are not greater than three so we stop to repeat the segmentation process. We extract the outer region of Fig. 1(c) and Fig 1(d) by skull elimination algorithm [14]. Thus by using the concepts of maximum connected area we can extract WM from segmented part of Fig. 1(c) and the result has been shown in Fig. 1(e). Thus Fig. 1(e) fully consist of WM has been shown below. The rest of the brain tissues are collected from Fig.1 (c) and combined with maximum connected area component of Fig. 1(d) to produce GM. GM has been shown in Fig. 1(f). After extracting GM from segmented Fig. 1(d), rest of the brain tissue part is consider as CSF. Fig. 1(g) fully consist of CSF has been shown below. The similar way muscle skin and marrow as non tissue part of the brain has been shown in Fig. 1(h) and Fig. 1(i) below. Thus we able to segment different brain tissues with some other non-brain region very efficiently and truthfully. Fig. 1 shows all the segmented region of MRI of brain below.

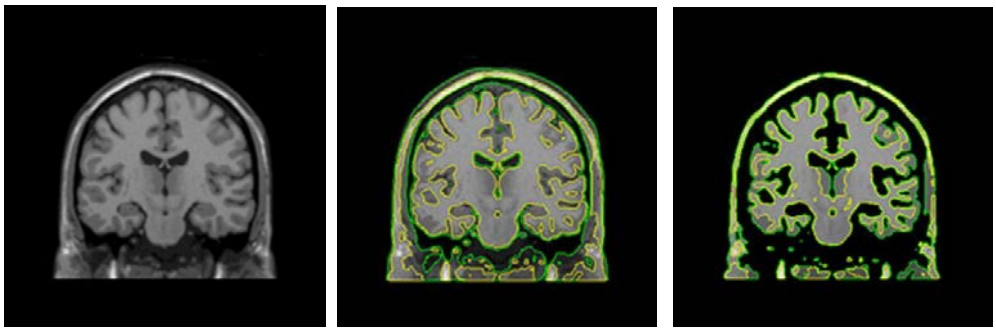

(a) (b) (c)

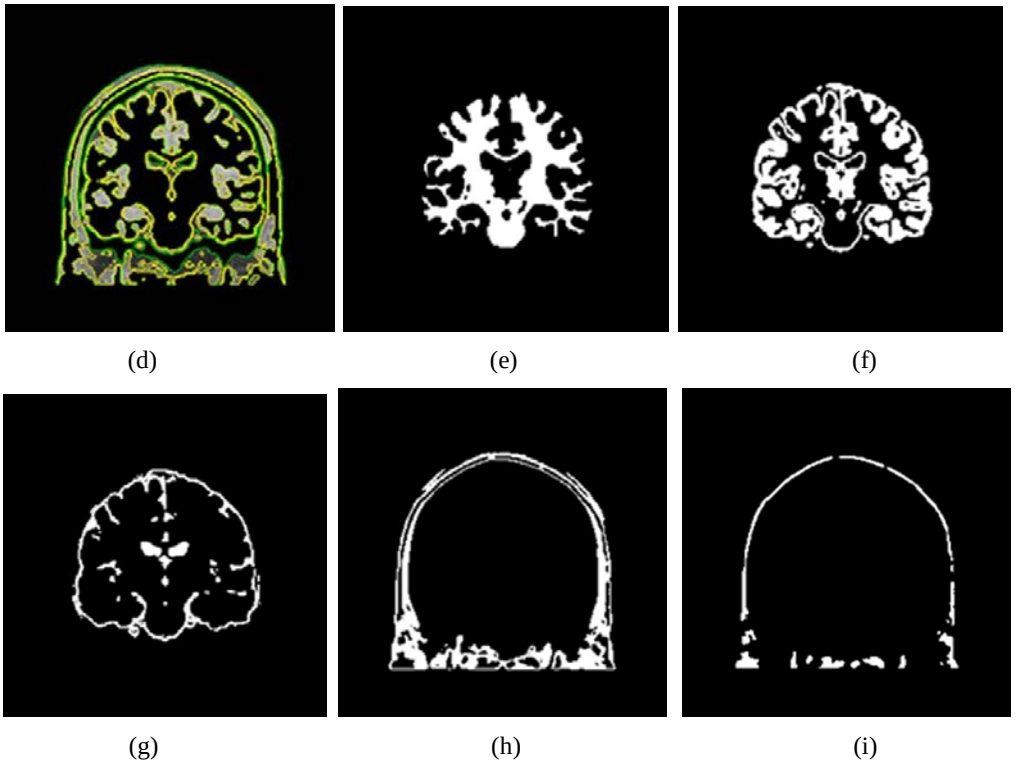

Fig. 1. (a) Input MRI image; (b) three phase level set output performed on input image; (c) and (d) are the outputs of level set performed on segmented region of (b); (e) is the segmented white matter; (f) is segmented gray matter; (g) is segmented CSF; (h) is segmented muscle skin; and (i) is segmented marrow region of brain

Our proposed method gives very good results for segmentation of different regions from the visualization point of reference. From the above figure it is easy to find out the area of each segmented region. The quantification and ratio of each segmented region such as WM, GM, and CSF has a great importance to identify the different type of brain disease. Different type abnormality has been also identified by their position on diverse brain tissues and dissimilar brain skull portions. Skull defect and appearances lesions may cause of skull meningeal and sulcal disease. Extracerebral masses and intracerebral masses can also been identified by our proposed method and abnormality detection [16] algorithm.

As segmentation may be biased visually thus we need to justify in terms of mathematical metric. Accuracy of a segmentation technique refers to the degree to which the segmentation results agree with the true segmentation. Although digital apparition can provide a level of recognized “ground truth or reference”, they are silently incapable to reproduce the full range of imaging characteristics and normal and abnormal anatomical variability observed in clinical data. First let AS be the automated segmented area and MS be the manual segmented area [16]. True positive TP is determine by the intersection pixel between automated (AS) and manual (MS) segmented area. False positive (FP) is determine by difference between AS and TP. False negative (FN) is determine by difference between MS and TP. The Jaccard index (J_i) between two areas is represented as follow:

$$J_i(AS, MS) = \frac{|AS \cap MS|}{|TP + FN + FP|} * 100\% \tag{6}$$

The relative area error (RAE) [16] for stroke region can be calculated as difference between ‘AS’ and ‘MS’ divided

by MS.

$$RAE = \frac{(AS - MS)}{MS} * 100\% \quad (7)$$

Jacard Index measures the similarity measurement between two images and RAE measure the relative area error between two images. Thus greater Jacard index means better results and lesser RAE means better results. The performance of our proposed method for different region segmentation with above mentioned metric has been shown in table 1.

Table 1.Performance measurement of segmented region

Segmented Region	Image Type	Segmented Area	Ground truth area	True Positive	False Positive	False Negative	Relative Area Error	Jacard Index
	Coronal	25828	25871	25578	293	250	0.1662	98.9496
	Coronal	25987	25467	25302	165	685	2.0418	98.3480
WM	Sagittal	16222	16854	16003	851	219	3.7498	96.7650
	Sagittal	17329	16897	16774	123	555	2.5566	98.0190
	Transverse	39272	38885	38428	457	844	0.9952	98.3354
	Transverse	36874	37843	36577	1266	297	2.5605	97.9081
	Coronal	27400	27947	27334	613	066	1.9572	98.7731
	Coronal	27438	27324	27287	037	151	0.4172	99.6566
GM	Sagittal	32478	35361	32349	3012	129	8.1530	95.3699
	Sagittal	35230	34657	34485	172	745	1.6533	98.6878
	Transverse	39121	43163	39004	4159	117	9.3645	94.8033
	Transverse	41857	42897	40468	2429	1389	2.4244	95.4951
	Coronal	10078	10017	10006	011	072	0.6089	99.1099
	Coronal	12008	11887	11835	052	173	1.0179	98.7907
CSF	Sagittal	38324	42057	38297	3760	027	8.8760	95.2886
	Sagittal	42482	41780	41632	148	850	1.6802	98.8155
	Transverse	16722	17829	16643	1186	079	6.2089	96.3387
	Transverse	19542	18907	18843	064	699	3.3585	98.0155
	Coronal	21784	21625	21543	082	241	0.7352	99.2559
	Coronal	20133	19876	19746	130	387	1.2930	98.7077
Muscle	Sagittal	20366	21205	19045	2160	1321	3.9566	91.6263
Skin	Sagittal	21758	22267	21566	701	192	2.2858	97.9716
	Transverse	18504	20240	18268	1972	236	8.5770	94.3010
	Transverse	19357	19876	19307	569	050	2.6111	98.4222
	Coronal	5360	5236	5200	036	160	2.3682	98.1502
	Coronal	5328	5276	5198	078	130	0.9855	98.0384
Marrow	Sagittal	8301	8602	8267	335	034	3.4991	97.8169
	Sagittal	8756	8538	8498	040	258	2.5532	98.2768
	Transverse	6895	7326	6798	528	097	5.8831	95.6050
	Transverse	7287	7485	7223	262	064	2.6452	97.7931

From the above table it is clear that Jacard index always reached greater than 90% where average value is 97.44789. Thus greater Jacard index means better segmentation procedure. Average value of RAE is 3.172822984 which are very less value. Relative area error is also very less in our proposed method. Thus our proposed method

produces high accuracy with low error rate which is very essential for medical image segmentation. Our method has more truthful results than what can be acquired with its individual modules. To produce much more competent segmentation method our framework detains dissimilar types of features in each step that are of particular significance for MRI, i.e., allotments of tissue intensities, textural features, and connection with adjacent pixels or spatial features. A most important benefit of this method is the use of spatial information. The tissue probability of a pixel is determined by the signal intensities and by the location of the pixels. The method segments tissues that are heterogeneous in signal intensity. Although we also embrace the control of intensity correlated issues of other part of brain due to the spatial features and this method is less sensitive to noise for it. Thus our method correctly segment visually as well as metrically for different type of MR images with different tissues.

4. Conclusion

The experimental results signify that our proposed segmentation methods can increase the overall segmentation performance with each component individually. This is because the proposed method takes advantages of the categorization ability of segmentation method in addition to the MR intensity. Level set framework has been used for three phase segmentation with a fixed number of regions; we described a way how to reach accuracy of results by using peak calculation concept. All advantages of the level set framework are conserved, while its main problem related to accuracy has been solved. Robustness to noise, low error rate and high accuracy are the advantages of proposed framework. In order to examine the proposed segmentation method, it has been used for brain tissue segmentation using standard dataset. The experiments demonstrated that the segmentation results are much closer to ground truth.

Acknowledgements

It is my privilege to thank Dr. Pradip Saha, is MD in Radiology from NRS Medical College and ex-Faculty from there. He is currently radiologist at M N Roy Diagnostic Center, Kolkata, India. He has supported for choosing reference images, guided, and given us the valuable suggestions to complete this paper which helps to enrich our knowledge.

References

1. Spinks R, Magnotta VA, Andreasen NC, Albright KC, Ziebell S, Nopoulos P. Manual and automated measurement of the whole thalamus and mediodorsal nucleus using magnetic resonance imaging. Neuroimage 2002;17:631‑42.
2. K. Van Leemput, F. Maes, D. Vandermeulen e P. Suetens. Automated Model-Based Tissue Classification of MR Images of the Brain. IEEE Transactions on Medical Imaging, vol. 18, n.º 10, pp. 897-98, 1999.
3. B. B. Avants, N. J. Tustison, J. Wu, P. A. Cook e J. C. Gee. An Open Source Multivariate Framework for n-Tissue Segmentation with Evaluation on Public Data. Neuroinformatics, pp. 381-400, 2011.
4. B. Fischl, D. H. Salat, E. Busa, M. Albert, M. Dieterich, C. Haselgrove, A. van der Kouwe, R. Killiany, D. Kennedy, S. Klaveness, A. Montillo, N. Makris, B. Rosen e A. M. Dale. Whole Brain Segmentation: Automated Labeling of Neuroanatomical Structures in the Human Brain. NeuroImage, vol. 33, pp. 341-355, 2002.
5. P. Aljabar, R. A. Heckemann, A. Hammers, J. V. Hajnal e D. Rueckert. Multi-atlas based segmentation of brain images: Atlas selection and its effect on accuracy. NeuroImage, vol. 46, pp. 726-738, 2009.
6. Z. Yi, A. Criminisi, J. Shotton e A. Blake. Discriminative, Semantic Segmentation of Brain Tissue in MR Images. Medical Image Computing and Computer-Assisted Intervention – MICCAI, vol. 5762, pp. 558-565, 2009.
7. Albert Huang, A., R. Abugharbieh. A Hybrid Geometric Statistical Deformable Model for Automated 3-D Segmentation in Brain MRI. Biomedical Engineering, IEEE Transactions on 56(7): 1838-1848, (2009).
8. Varghese, T., R. S. Kumari. Discrimination between Alzheimer's Disease, Mild Cognitive Impairment and Normal Aging Using ANN Based MR Brain Image Segmentation. Proceedings of the International Conference on Frontiers of Intelligent Computing: Theory and Applications (FICTA) 2014, Springer.
9. Agrawal, R. and M. Sharma. Review of Segmentation Methods for Brain Tissue with Magnetic Resonance Images. International Journal of Computer Network and Information Security (IJCNIS), 6(4): 55. (2014)
10. Kilian M. Pohl, Sylvain Bouix, Ron Kikinis, W. Eric L. Grimson. Anatomical Guided Segmentation with Non-Stationary Tissue Class Distributions In An Expectation-Maximization Framework. 2004 IEEE International Symposium on Biomedical Imaging: From Nano To Macro, Arlington, VA.
11. S. Osher and J. A. Sethian. Fronts propagating with curvature dependent speed: Algorithms based on Hamilton-Jacobi formulations. Journal of Computational Physics, vol. 79, no. 1, pp. 12–49, 1988.

12. Chunming Li, Rui Huang, Zhaohua Ding, J. Chris Gatenby, Dimitris N. Metaxas. A Level Set Method for Image Segmentation in the Presence of Intensity Inhomogeneities With Application to MRI. IEEE Transactions On Image Processing, VOL. 20, NO. 7, JULY 2011
13. N. Paragios and R. Deriche. Coupled geodesic active regions for image segmentation: A level set approach. In European Conference in Computer Vision, pp. 224–240, Springer, 1999.
14. S Roy, S Nag, I K Maitra, S K Bandyopadhyay. Artefact Removal and Skull Elimination from MRI of Brain Image. International Journal of Scientific and Engineering Research, Volume 4, Issue 6, June-2013, pp 163-170.
15. http://brainweb.bic.mni.mcgill.ca/brainweb/ (May 2013)
16. S Roy, S Nag, S K Bandyopadhyay, D Bhattacharyya, T Kim. Automated Brain Hemorrhage Lesion Segmentation and Classification from MR Image Using an Innovative Composite Method. Journal Of Theoretical And Applied Information Technology, Volume 78, No. 1, pp. 34-45, August, 2015 Issues.